JOURNAL OF MATERIALS SCIENCE 4 (1969) 861–872

Precipitate Strengthening Mechanisms in Magnesium Zinc Alloy Single Crystals

J. S. CHUN, J. G. BYRNE
Division of Materials Science and Engineering, University of Utah, USA

Received 14 April 1969

The mechanical behaviour of Mg–5.1 wt % Zn alloy single crystals was studied in the 4.2 to 300° K temperature range. Quenched crystals have activation energies and volumes best associated with the cutting of small clusters of Zn atoms by dislocations. Fully hardened crystals contain fine β_1' and occasional β_2' precipitates with an average β_1' interparticle spacing of 330 to 660 Å. Strengthening in these crystals is mainly ascribed to the cutting of β_1' particles by dislocations. In the overaged condition β_1', β_2' and equilibrium β particles are present and lead to a considerable temperature-dependence unusual for an overaged condition. Analysis of this temperature-dependence suggests that below 77° K the relatively easy cutting of β_1' particles by dislocations takes place in addition to the cutting of β_2' and β particles. Above 77° K the difficult cutting of β_2' and β particles alone controls the deformation, β_1' being more easily cut with the aid of thermal fluctuations.

1. Introduction

Much progress toward understanding strengthening mechanisms has been made by the use of fcc alloy single crystals. This approach was recently applied to hcp alloy single crystals of composition Mg + 1.33 wt % Mn [1–3]. This system is capable of relatively little age-hardening because the only precipitate which forms is the equilibrium one.

The present research was based on a binary Mg–Zn alloy since this system shows more hardening promise than the other Mg systems available [4]. Gallot [5] reported that two transition phases, β_1' and β_2', appeared prior to the appearance of the equilibrium β phase. β_1' and β_2' have the same Laves phase $MgZn_2$ structure but they differ in orientation as indicated in table I. Gallot concluded that GP zones do not form in the Mg–Zn system.

The temperature-dependence of the critical resolved shear stress (crss) of single crystals has been determined from 4.2 to 300° K for as-quenched, slightly aged, fully aged and overaged conditions. The temperature-dependence of Young's modulus and the strain-rate sensitivity of the flow stress were also determined. Direct

TABLE I Mg–Zn alloy parameters and orientation relationships of β_1', β_2' and β with the Mg matrix

Phase	Structure	Parameters	Orientation with matrix
Matrix (Mg)	hcp	$a = 3.2$ Å $c = 5.2$ Å $c/a = 1.624$	
β_1'*	Laves $MgZn_2$ type (hexagonal lattice)	$a = 5.2$ Å $c = 8.5$ Å	$[2\bar{1}\bar{1}0]\ \beta_1' \parallel [0001]$ Mg $[0001]\ \beta_1' \parallel [2\bar{1}\bar{1}0]$ Mg
β_2'*	Laves $MgZn_2$ type (hexagonal lattice)	$a = 5.2$ Å $c = 8.48$ Å	$[0001]\ \beta_2' \parallel [0001]$ Mg $[2\bar{1}\bar{1}0]\ \beta_2' \parallel [10\bar{1}0]$ Mg
β'*	Mg_2Zn_3 (triclinic)	$a = 17.24$ Å $\alpha = 96°$ $b = 14.45$ Å $\beta = 89°$ $c = 5.2$ Å $\gamma = 138°$	random

*Data from Gallot [5].

observations of the size, shape and distribution of the precipitates were made by transmission electron microscopy. Surface observation of slip traces were made by optical microscopy.

In addition to removing the complicating influence of grain-boundaries, research on alloy single crystals of hcp structure makes it possible in large part to isolate twinning effects from slip effects by choosing particular crystal orientations.

2. Experimental

2.1. Specimen Preparation

Single crystals several inches long and 0.33 by 0.98 cm in cross-section were grown from the melt by a modified Jillson [6] technique. Details of this method are described elsewhere [7]. Crystal orientations were determined by the Laue back-reflection method.

Gauge lengths were produced by electro-polishing after prior heat-treatment.

2.2 Heat-Treatments

2.2.1. Supersaturated Solid-Solution

Three days at 420° C in an SO_2 atmosphere, followed by a rapid quench into water was used. A temperature of 420° C (76° above the eutectic temperature) was found to be necessary for the single crystals. This contrasts with the 315° C temperature which Clark [8] found adequate for polycrystalline foil of the same composition. This is probably accounted for by the absence of grain-boundary diffusion in the present case.

2.2.2. Fully Aged Specimens

Twenty-eight hours at 200° C in an SO_2 atmosphere, followed by air-cooling.

2.2.3. Overaged Specimens

One thousand, four hundred and forty hours at 240° C in an SO_2 atmosphere, followed by air-cooling.

2.3. Testing

Rockwell E hardness tests were made immediately after ageing. Each reported value represents the average of eight measurements.

The temperature-dependence of Young's modulus was determined by a resonant dynamic method.

Tensile tests were performed with an Instron tensile testing machine in the same manner as described previously [2, 3]. The only procedural change made was for testing at 4.2° K. In the previous work [2, 3] the specimen was soldered to the grips. In the current work friction grips were used because of soldering difficulties with this alloy.

Load-elongation data were converted into resolved shear stress and glide strain following the computer program outlined by DeLuca [9].

Direct observations of the size, shape and distribution of the precipitate particles were made by transmission electron microscopy. Thin foils for transmission electron microscopy were made from 0.13 mm thick sheet material provided by the Dow Metal Products Company. The thinning procedure was that used by Clark [8].

3. Results

3.1. Hardness

Polycrystalline data for various ageing times at 100, 200 and 240° C are shown in fig. 1. Hardness increases slowly during the ageing at 100° C compared with ageing at 200 or 240° C. The maximum hardness occurs after ageing from 10 to 50 h at 200° C.

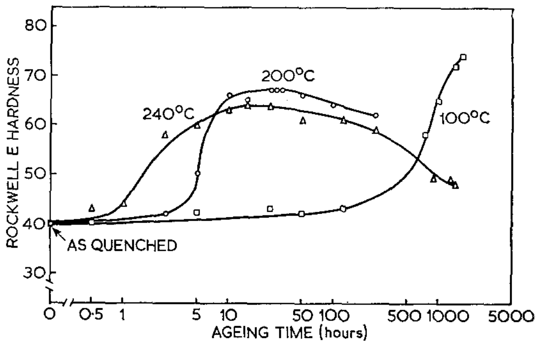

Figure 1 Rockwell E hardness as a function of ageing time and temperature for polycrystalline samples solution treated three days at 420° C.

Hardness was found to decrease very slowly at 240° C after the maximum. Hardness values in the region between 900 and 1440 h were approximately constant. This either indicates that a stable precipitate configuration was reached in this region or that the rate of transformation was very slow, indeterminately long ageing times being necessary to obtain complete transformation to the equilibrium phase. Thus, for the overaged condition, a time of 1440 h at 240° C was used. The proper ageing time at 200° C for maximum strength was determined with the aid of crss measurements at room temperature on five single crystals of similar orientation. Fig. 2

shows that maximum strength occurred at an ageing time of approximately 28 h.

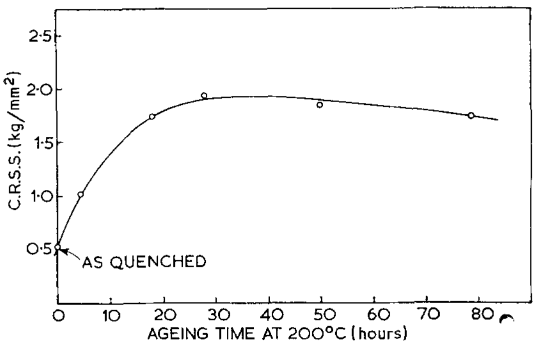

Figure 2 Critical resolved shear stress as a function of ageing time at 200° C.

3.2. Microstructure

The microstructures of thin foils representing the fully aged, overaged and slightly aged conditions were examined by transmission electron microscopy.

A typical microstructure for the fully aged condition is shown in fig. 3a. Most of the precipitates present were long, rod-like β_1' particles oriented perpendicular to the basal plane of the Mg matrix. The width of the β_1' precipitates was approximately 150 to 300 Å. The length was greater than this but difficult to determine precisely because of limitations due to the orientation of the crystal and the thickness of the sample. Ratios of length to width of up to 20 were measured for the β_1' precipitates. Relatively few short, rod-like β_2' precipitates were found to be present. Fig. 3b shows a typical field obtained with the electron beam normal to the basal plane of the Mg matrix. The average value of the interparticle spacing was approx. 330 to 660 Å. The calculated particle density was in the range of about 1 to 10^{15} per cm^3.

Fig. 4 is a typical microstructure after ageing 1440 h at 240° C viewed along [$\bar{1}$102]. In this figure β_1', β_2' and the equilibrium β precipitates are all present. Gallot [5] also reported that Mg–6.0 wt % Zn specimens aged 2160 h at 250° C contained β_1', β_2' and equilibrium β phase precipitates. Fig. 4 suggests that most of the β particles grew from the end of β_1' rod-like precipitates. Fig. 5 shows that β_2' precipitates also probably grow from the end of the β_1' rod-like precipitates and are oriented perpendicular to the β_1' rods. From these micrographs the average value of the interparticle spacing lies approximately between 2500 and 3500 Å and the total density of particles is about 2 to 5×10^{15} cm^3. The width of a typical β_2' precipitate is 300 to 500 Å. Length-to-width ratios of up to 20 have been measured for β_2' precipitates.

GP zones could not be detected by transmission electron microscopy in samples aged for various times up to 114 h at 100° C. Clark [8] has also reported that GP zones are not seen by transmission electron microscopy, even after ageing 500 h at 100° C. More recently, Gallot also reported the absence of GP zones.

3.3. Young's Modulus

Young's moduli values were obtained from acoustic spectrometer measurements between 77 and 300° K. The values of Young's modulus E and the rigidity modulus G, are listed in table II. These values were used to correct the temperature-dependence of the flow stress.

3.4. Temperature-Dependence of the crss

The variation of crss with temperature for single crystals with orientations centrally located in the stereographic triangle is shown in fig. 6. It is clear that a large temperature-dependence exists for all conditions. The temperature-dependence of the overaged condition below 77° K is exceptional. The fully aged condition shows a smaller temperature-dependence than either the quenched or overaged condition.

3.5. Strain-Rate Transitions During Deformation

The strain-rate dependence of the flow stress is shown in figs. 7, 8, and 9. Fig. 7 shows that $\Delta\tau$ at 77° K is larger than at 300° K. This is also evident in fig. 9. Fig. 8 shows that $\Delta\tau$ increases as the temperature is raised from 4.2 to 300° K.

3.6. Stress-Strain Curves for Single Crystals

Fig. 10 shows typical room-temperature stress-strain curves for all conditions of heat-treatment. The minimum rate of work-hardening for the quenched condition is 2.5×10^{-4} G. This value is similar to the value of 1.5×10^{-4} G, obtained for pure magnesium single crystals [10]. Fully aged crystals exhibit work-hardening rates of 5.4 to 5.7×10^{-4} G. These values are of the same order of magnitude as those for quenched crystals. The overaged condition has a rate of work-hardening of 7.4×10^{-4} G which is much

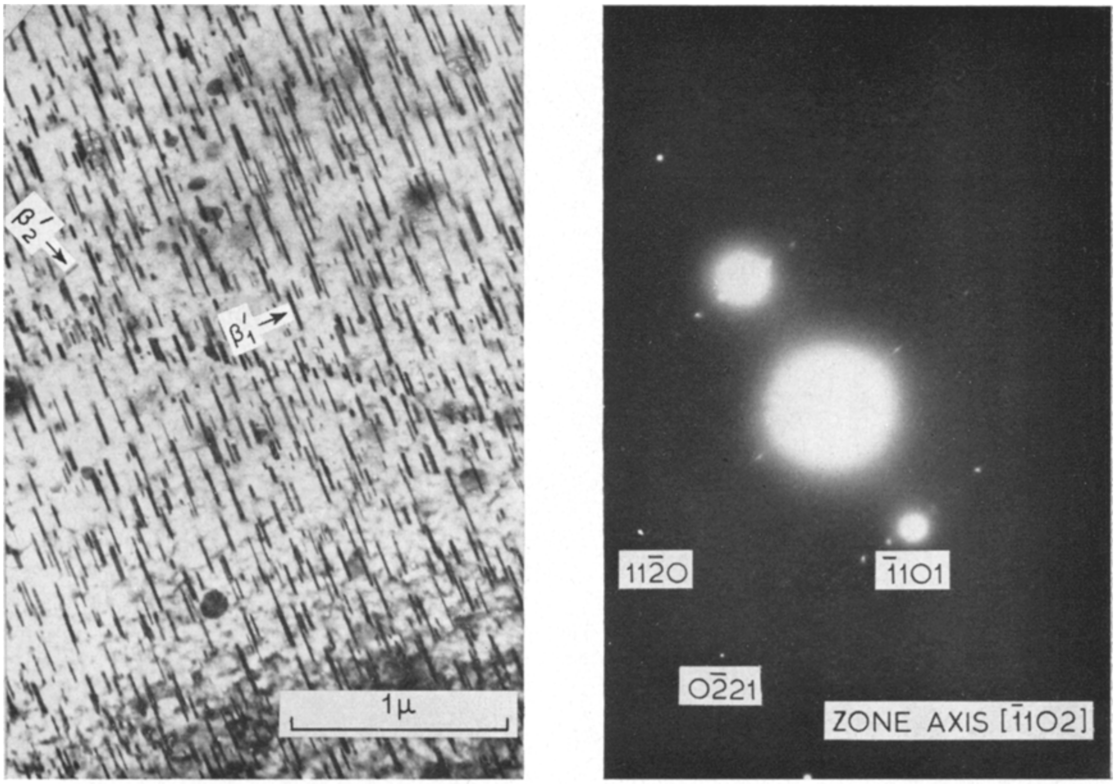

(a)

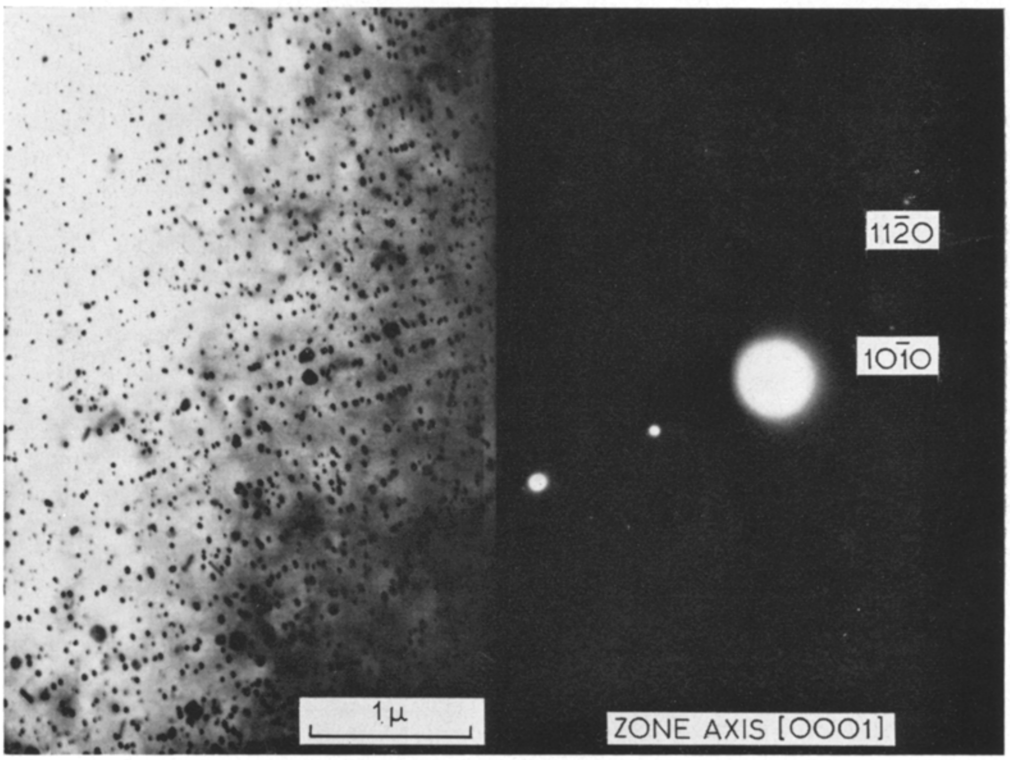

(b)

Figure 3 Transmission electron micrograph and diffraction pattern of sample aged 28 h at 200° C. (a) Viewed along [$\bar{1}$102]. (b) Viewed along [0001].

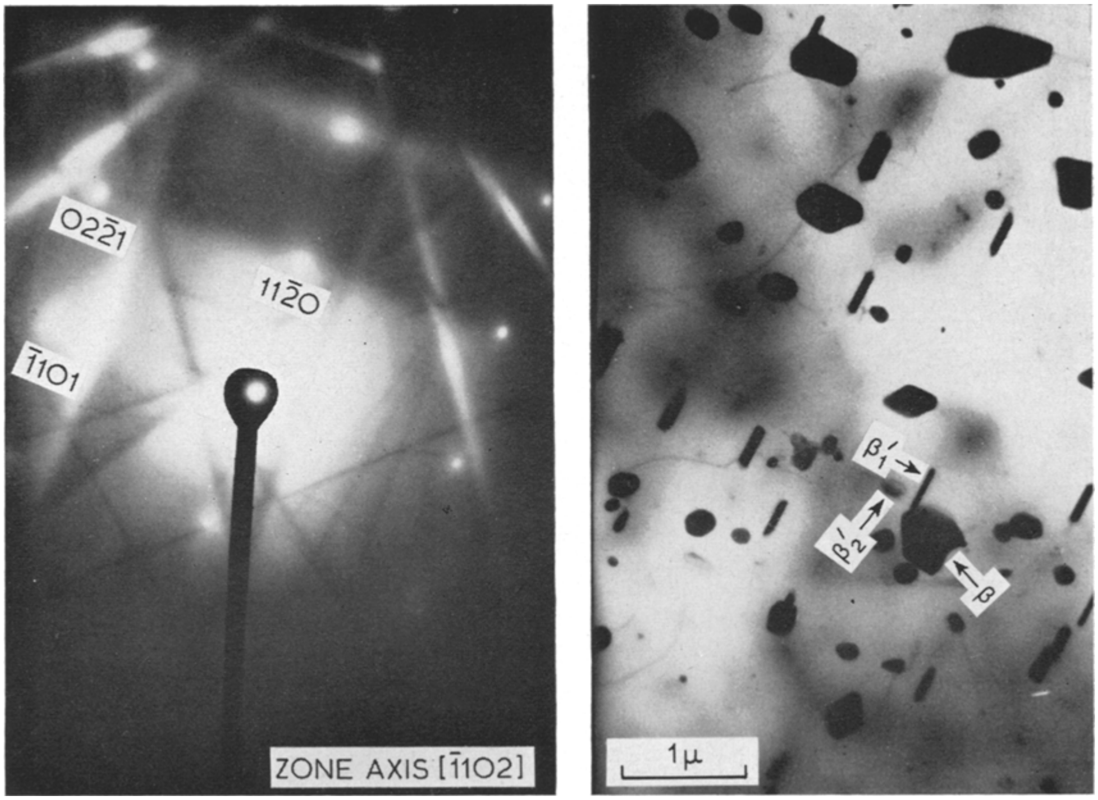

Figure 4 Transmission electron micrograph and diffraction pattern of sample aged 1440 h at 240° C showing dislocations.

like that for the fully aged condition. Fig. 10 shows that the stress-strain curve for the overaged condition is linear after approximately 5 to 10% glide strain, whereas the stress-strain curve for the fully aged crystal is concave.

Fig. 11 shows typical single crystal curves at 77° K. The rates of work-hardening for all conditions of heat-treatment are within the range of 1×10^{-4} G to 17×10^{-4} G. The shape of the fully aged and overaged crystal curves is similar to that of those at room temperature.

Fig. 12 shows that the rates of work-hardening for all conditions were similar at 4.2° K. The values fall between 2.6×10^{-4} G and 4.3×10^{-3} G. The range of strain over which twinning serrations occur in load deflection curves is noted by the dashed lines. The total glide strain for the overaged and fully aged crystals shown in fig. 12 is 76 and 30%, respectively, compared with 10% for the quenched crystal.

Tensile axis rotations were determined by obtaining Laue patterns after fracture. Laue spots for crystals deformed at room temperature have a small amount of asterism. This increases as the temperature is decreased and depends more on temperature than on the ageing condition.

Slip lines of quenched crystals are finer and

TABLE II Young's modulus (E) and the shear modulus (G) as a function of temperature

Condition	E dynes/cm^2			G dynes/cm^2		
	300° K	198° K	77° K	300° K	198° K	77° K
Quenched	4.00×10^{11}	4.21×10^{11}	4.36×10^{11}	1.56×10^{11}	1.64×10^{11}	1.70×10^{11}
Fully Aged	4.22×10^{11}	4.35×10^{11}	4.54×10^{11}	1.65×10^{11}	1.70×10^{11}	1.78×10^{11}
Overaged	3.88×10^{11}	4.04×10^{11}	4.14×10^{11}	1.51×10^{11}	1.58×10^{11}	1.62×10^{11}

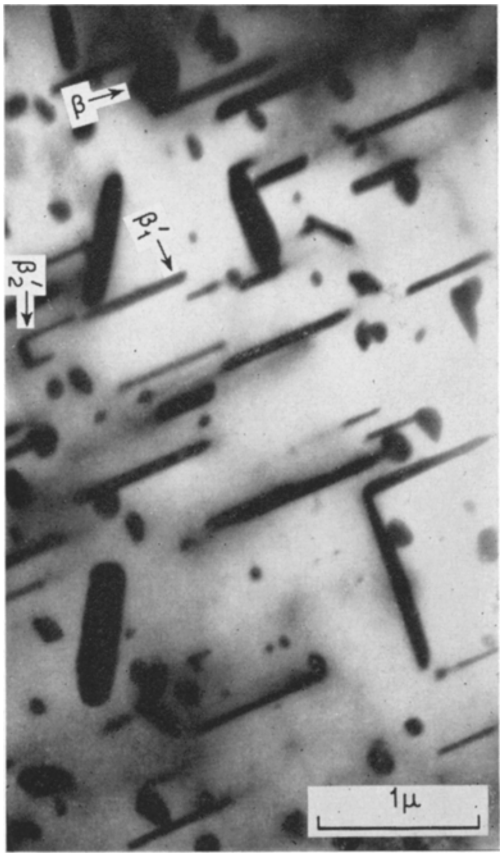

Figure 5 Transmission electron micrograph of sample aged 1440 h at 240° C showing β_1'–β_2' relationship.

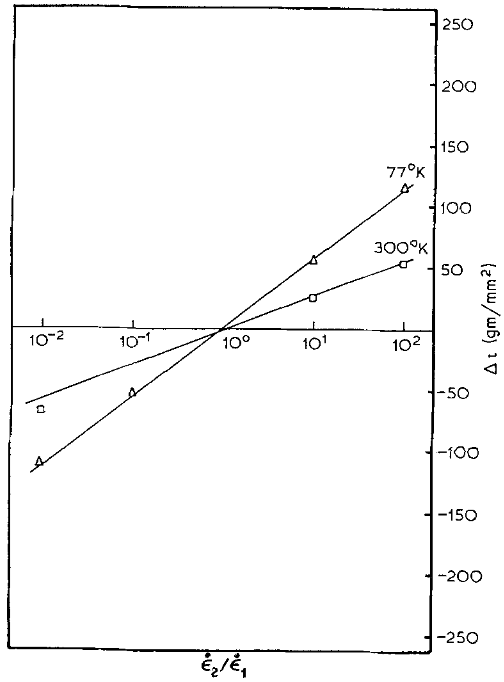

Figure 7 The change in flow stress accompanying a change in strain rate for quenched single crystals.

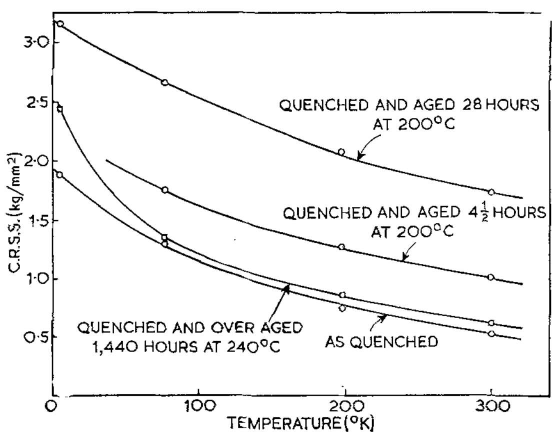

Figure 6 Critical resolved shear stress as a function of temperature.

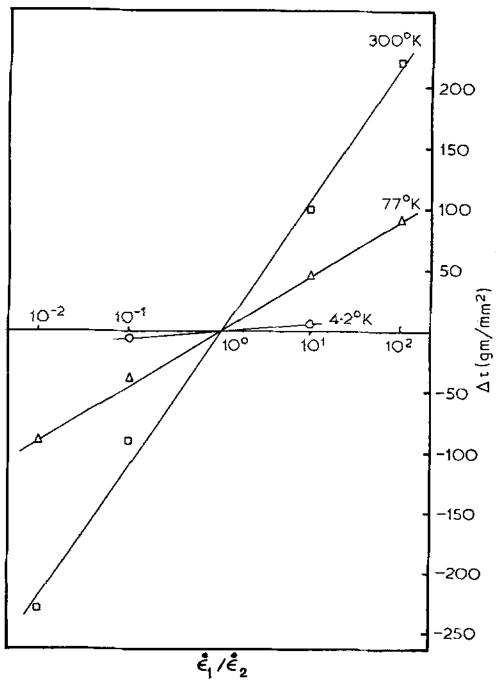

Figure 8 The change in flow stress accompanying a change in strain rate for fully aged single crystals.

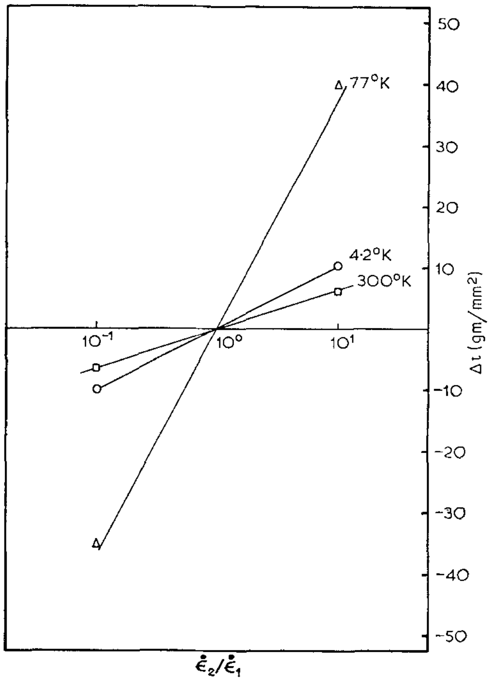

Figure 9 The change in flow stress accompanying a change in strain rate for overaged single crystals.

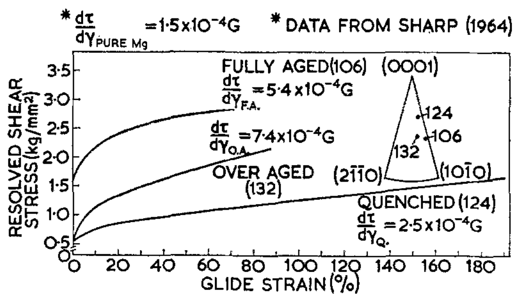

Figure 10 Resolved shear stress versus glide strain for single crystals deformed at room temperature. Initial orientations are indicated in the stereographic triangle.

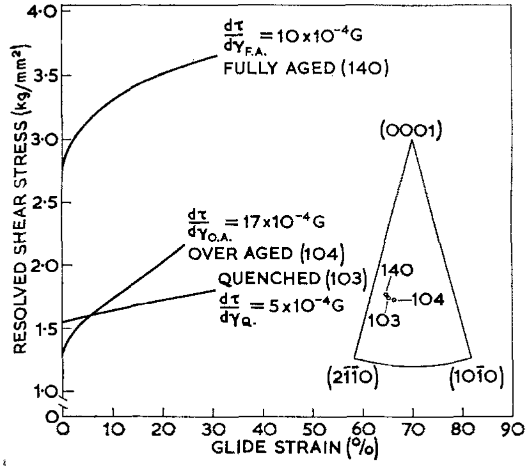

Figure 11 Resolved shear stress versus glide strain for single crystals deformed at 77° K. Initial orientations are indicated in the stereographic triangle.

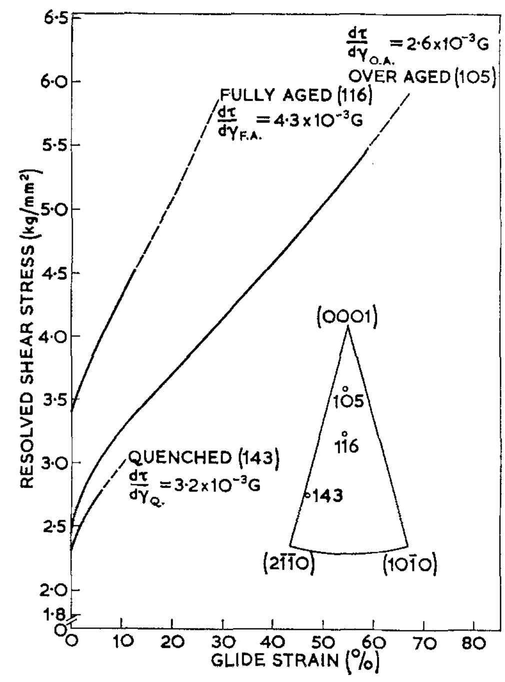

Figure 12 Resolved shear stress versus glide strain for single crystals deformed at 4.2° K. Initial orientations are indicated in the stereographic triangle.

more closely spaced than for fully aged crystals. In overaged crystals, slip lines were not observed with light microscopy. Difficulty of observation of slip lines has also been noted in the Al–Cu system [11] in the presence of GP II zones and in overaged crystals of the Mg–Mn system [9].

4. Discussion

4.1. The Mechanism of Strengthening for the Quenched Condition

Considerable temperature-dependence of the crss for quenched crystals remains after correcting for the temperature-dependence of the shear modulus, as is evident from fig. 13. This temperature-dependence is similar to that of the reverted

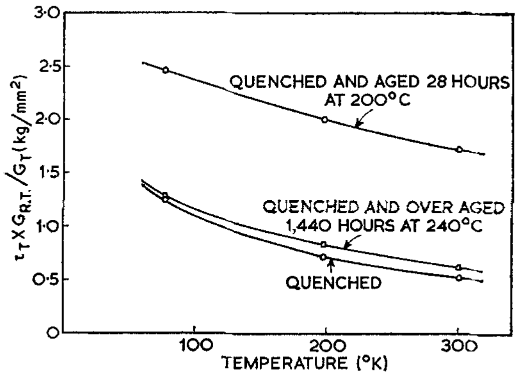

Figure 13 The temperature-dependence of the critical resolved shear stress corrected for the variation of the shear modulus with temperature for single crystals aged various amounts after a solution-treatment of three days at 420° C.

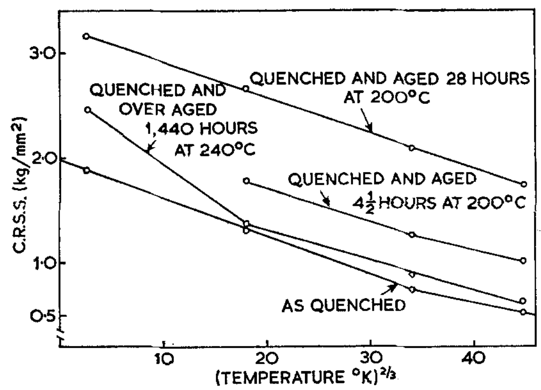

Figure 14 Critical resolved shear stress as a function of $T^{2/3}$ for various heat-treatments.

state of Al–3.9 wt % Cu [11]. In that case it was concluded that the low-temperature strengthening was due to the cutting of small clusters of Cu atoms by dislocations. The Mott and Nabarro theory [12] for solid-solution hardening gives the crss as:

$$\tau = 2.5\mu\epsilon^{4/3}c\,,$$

where c is the atomic concentration of solute, ϵ is the fractional difference in size between the solute and solvent atom ($\epsilon = 0.1488$ for Zn in Mg) and μ is the shear modulus ($\mu = 1.56 \times 10^{11}$ dyne/cm² at RT). Then τ would be 6.62 kg/mm², which is almost 12 times larger than the experimental value of 0.52 kg/mm². Fisher's short-range order strengthening [13] and Suzuki strengthening [14] can be ruled out as mechanisms because neither predicts the large temperature-dependence observed.

Friedel's [15] model predicts a linear decrease of crss with T; Cottrell's [16] model predicts a linear decrease of crss with $T^{1/3}$; and Fleischer's [17] model gives a linear decrease of (crss)$^{1/2}$ with $T^{2/3}$. A theory combining conclusions of Mott [18] and Seeger [19] was shown to apply to dislocation-precipitate interactions [11, 20]. This theory predicts a linear dependence between crss and $T^{2/3}$.

The temperature-dependence of the crss was analysed on the basis of all these models. The best agreement between data and theory occurred for the crss versus $T^{2/3}$ relationship. Such a plot is shown in fig. 14. The crss of quenched crystals follows two linear branches as also was found in the Mg–Mn system [21].

According to this theory, the relationship between the crss, τ, and the activation energy, U_0, is:

$$\tau = \frac{U_0}{v}\left\{1 - \left[\frac{kT}{U_0}\ln\left(\frac{\dot\epsilon_0}{\dot\epsilon}\right)\right]^{2/3}\right\} \qquad (1)$$

in which v is the activation volume, $\dot\epsilon$ is the strain rate, $\dot\epsilon_0 = NA\mathbf{b}\nu_0$ (N = number of obstacles per unit volume, A is the area of slip plane swept out per activated event, **b** is the Burgers vector of the dislocation and ν_0 is the vibrational frequency of a dislocation against an obstacle) and k and T have their usual meanings. When $\tau = 0$ it follows that:

$$U_0 = kT_c \ln\left(\frac{\dot\epsilon_0}{\dot\epsilon}\right) \qquad (2)$$

i.e. at a critical temperature T_c, the flow stress due to this barrier becomes zero. For the low-temperature branch the slope for the quenched condition is:

$$\frac{d\tau}{dT^{2/3}} = \frac{U_0^{1/3}}{v}\left(k\ln\frac{\dot\epsilon_0}{\dot\epsilon}\right) = 3.65 \times 10^{-2}\ \text{kg/mm}^2\,(^\circ\text{K})^{2/3}. \qquad (3)$$

At $T = 0°$ K, $\tau = U_0/v$ from equation 1 and the appropriate value of τ is obtained by subtracting 1.46 kg/mm² (intercept at 0° K of the extrapolated high-temperature branch) from the 0° K intercept of the low-temperature branch in fig. 14, i.e.

$$\frac{U_0}{v} = 1.98 - 1.46 = 0.52\ \text{kg/mm}^2\,.$$

Fig. 7 shows the strain-rate sensitivity of flow stress. At 77° K this is:

$$\frac{d\tau}{d\ln\dot\epsilon} = 2.35 \times 10^{-2}\ \text{kg/mm}^2\,.$$

Combining the last three expressions with the equation for U_0 gives an activation energy, U_0, of 0.31 eV and an activation volume, v, of

$$9.8 \times 10^{-21}\,\mathrm{cm}^3 .$$

It seems likely that the low-temperature strengthening in quenched crystals is due to the cutting of small clusters of Zn atoms by dislocations. Some clustering is to be expected in this alloy on the basis of the 20% difference in atom size between Mg and Zn. Clark [8], for example, has observed small dislocation loops in solution-treated samples of Mg–5.0 wt % Zn alloy quenched from 315° C. As vacancies migrate through the lattice to form dislocation loops, they may bring solute atoms with them. Under these conditions, the solute atoms may segregate to form very small clusters. Experimental evidence in favour of this view in Al alloys has been obtained by Desorbo *et al* [22], Federighi [23], and Turnbull and Rosenbaum [24] who measured changes in electrical resistivity immediately after quenching. Hirsch and Kelly [25] predicted that if an alloy has segregated into clusters and the stacking-fault energy in the clusters is less than in a matrix dislocations will tend to pass through as many particles as possible. Since the stacking-fault energy of Zn is approximately 15 ergs/cm² [26] and that for Mg is approximately 60 ergs/cm² [27] the Kelly-Hirsch theory would suggest that the low-temperature strengthening mechanism is the cutting of small clusters of Zn atoms by dislocations.

The stress-strain curves of quenched crystals were very similar in shape to those of pure Mg single crystals at 4.2, 77 and 300° K [28]. This curve shape for quenched crystals was also found in the Mg–Mn system [2] and in the Al–Cu system [11]. The latter paper indicated that solute elements mainly affect the crss and not the rate of work-hardening provided the crystal is deformed at temperatures too low for precipitation or clustering to occur during the deformation.

No definite conclusion can be made in regard to the sources of the strengthening in the temperature range 198 to 300° K where the crss varies only a small amount with temperature.

4.2. The Mechanism of Strengthening for the Fully Aged Condition.

Considering the large variation of the crss with temperature shown in fig. 6, the temperature-dependence is still large after correction for the temperature-dependence of the shear modulus. This contrasts with the results of Clark [8] who showed virtually no such temperature-dependence for Mg–5.0 wt % Zn polycrystals. The current results indicate the presence of a thermally activated process. Reasons for this difference in results between single and polycrystal tests are proposed elsewhere [29]. They involve textures and deformation twinning which depart from present considerations.

Again, the experimental observations are best correlated with the combination of Mott's and Seeger's theories requiring that the crss vary linearly with $T^{2/3}$. In fig. 14 the crss values of fully aged crystals do fall on a straight line as predicted.

Consideration of fig. 8 shows that $\Delta\tau$ increases continuously with increasing temperature as the above theory predicts. The equation

$$\frac{\mathrm{d}\tau}{\mathrm{d}\ln\dot{\epsilon}} = \frac{(kT)^{2/3}\,U_0^{1/3}}{\frac{3}{2}v\left[\ln\frac{\dot{\epsilon}_0}{\dot{\epsilon}}\right]^{1/3}}, \tag{4}$$

obtained by differentiating equation 1, indicates that $\mathrm{d}\tau/\mathrm{d}\ln\dot{\epsilon}$ is a linear function of $T^{2/3}$. This is substantiated in fig. 15. Assuming that the critical temperature, T_c, is 300° K then from fig. 14, the difference between the 0° K intercept and the crss at 300° K is:

$$\frac{U_0}{v} = 1.52\ \mathrm{kg/mm^2} .$$

From the slope of the τ versus $T^{2/3}$ curve (fig. 14)

$$\frac{\mathrm{d}\tau}{\mathrm{d}T^{2/3}} = 3.39 \times 10^{-2}\ \mathrm{kg/mm^2}\,(^\circ\,\mathrm{K})^{2/3} .$$

Solving equation 3 with the values of $\mathrm{d}\tau/\mathrm{d}\ln\dot{\epsilon}$ at different temperatures, values for $\ln \dot{\epsilon}_0/\dot{\epsilon}$ of 24.7, 22.4 and 19.3 for temperatures of 300, 77 and 4.2° K, respectively are obtained. Substituting

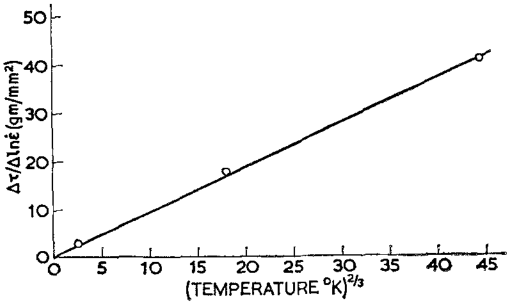

Figure 15 Strain-rate sensitivity of the flow stress ($\Delta\tau$/ d$\ln\epsilon$) for fully aged single crystals as a function of $T^{2/3}$.

these values of $\ln \dot{\epsilon}_0/\dot{\epsilon}$ into equation 2 for U_0, results in activation energies between 0.5 and 0.65 eV and activation volumes between 5 and 7×10^{-21} cm^3.

Fig. 3 showed that most of the precipitates present are long, rod-like β_1' particles oriented perpendicular to the basal plane of the matrix. The associated interparticle spacing is 330 to 660 Å compared to the 1000 to 2000 Å spacing reported by Clark [8]. This may arise from the use of a higher solution-treating temperature in the present study (see section 2.2.3). Although the solubility limit at 420° C is not appreciably different from that at 315° C, the vacancy concentration and the diffusivity of Zn in Mg should be greater.

The theoretical value for the activation volume can be computed and compared with the experimental value. The theoretical activation volume is given [11, 19] as:

$$v_{\text{calc.}} = 4\mathbf{b}l_0X_0 \qquad (5)$$

where **b** is the Burgers vector of dislocation, l_0 is the interparticle spacing of the precipitates and X_0 is the distance moved per activated event.

If one assumes that a dislocation moves forward a distance **b**, then

$$v_{\text{calc.}} = 4\mathbf{b}^2l_0\,.$$

Letting $\mathbf{b} = 3.2$ Å and $l_0 = 330$ Å, the calculated activation volume is 13.5×10^{-21} cm^3, which compares favourably with the experimental value of 5 to 7×10^{-21} cm^3.

Fig. 16 shows the orientation relationship between the β_1' precipitate and the Mg matrix. The basal plane of the β_1' is perpendicular to the basal plane of the Mg matrix, however, the plane of the highest atomic density in the β_1' precipitate is $(2\bar{1}\bar{1}0)$. Thus dislocations in the Mg basal plane should easily cut through the β_1' precipitates. This lends support to the shear mechanism in the fully aged condition.

The minimum rate of work-hardening at room temperature for the fully aged condition was

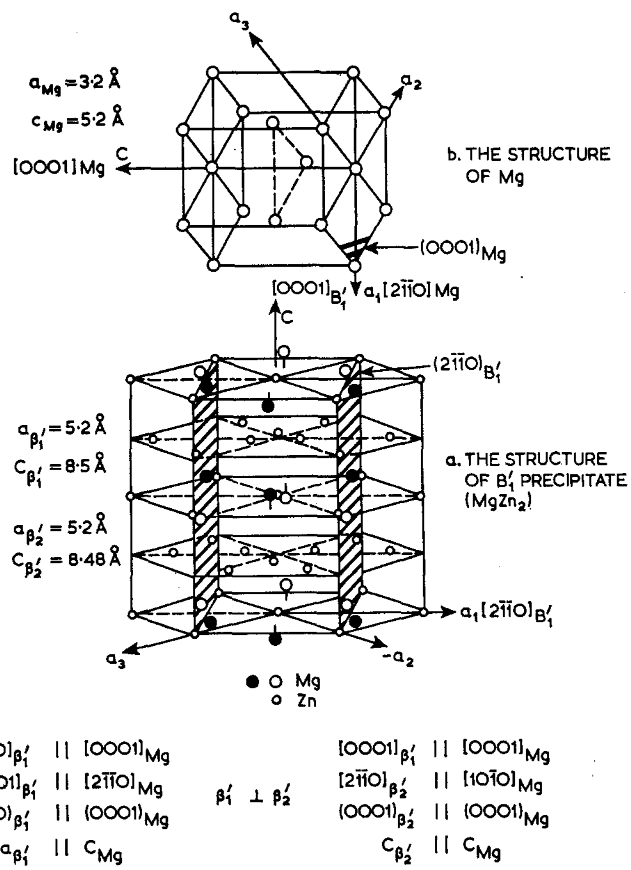

Figure 16 Orientation relationships between β_1' and the Mg matrix.

about the same as for the quenched condition and for pure Mg. At 77 and 4.2° K, the minimum rate of work-hardening for the fully aged crystal was the same order of magnitude as for the quenched crystal. A similar case exists in Al–3.9 wt % Cu alloy [11] where the dislocations sheared the precipitates.

Clark [8] suggested that the strengthening he observed is explained by Orowan's [30] theory which enables one to calculate the crss utilising a model in which the applied force does work in bowing dislocations between precipitate particles.

Using an interparticle spacing, L, of 330 Å, in the Orowan formula:

$$\tau_{\text{calculated}} = \tau_{\text{solid solution}} + \frac{2G\mathbf{b}}{L} \quad (6)$$

together with

$\tau_{\text{ss}} \simeq 0.52$ kg/mm^2 (present data at 300° K)
$G \simeq 1.680$ kg/mm^2 (present data at 300° K)
$\mathbf{b} \simeq 3.3$ Å

one obtains

$$\tau_{\text{calc.}} = 33.12 \text{ kg/mm}^2 .$$

The observed value 1.73 kg/mm^2 (300° K) therefore makes it appear quite unlikely that the Orowan mechanism is active.

All of the present experimental results indicate that in fully aged crystals, the mechanism of strengthening is the cutting of MgZn′ precipitates by dislocations, rather than the bowing of dislocations between the precipitates.

4.3. The Mechanism of Strengthening for an Overaged Condition

On the basis of the close similarity between the features in fig. 5 and those in Gallot's work [5] it is concluded that β_1', β_2' and β were all present in specimens aged for 1440 h at 240° C.

Gallot [5] reported that the β-phase is triclinic Mg_2Zn_3 coherent with the Mg matrix with numerous epitaxial relationships possible. The variation of crss with temperature is shown in fig. 6 and after correction for G in fig. 13 indicates the presence of a thermally activated process. In fig. 14, two linear branches are observed which implies that there are two barrier types in the overaged condition. Assuming that the critical temperatures are 77 and 300° K for the low- and high-temperature branches respectively and that equation 1 holds for both barriers, then from the Mott and Seeger analyses, activation energies U_0 of 0.37 eV and 7.68 eV are obtained. Activation volumes v of 7.6×10^{-21} cm^3 and 7.68×10^{-20} cm^3 were calculated for the low- and the high-temperature branches, respectively.

The experimental value of 0.37 eV for the low-temperature branch agrees well with values obtained for the fully aged crystals. In these the cutting of β_1' precipitates is the deformation mechanism. The slightly increased activation volume and the decreased activation energy in the overaged condition are probably due to the partial dissolution of β_1' to form β_2' and β, resulting in a lower value of crss than for the fully aged condition.

The activation energy associated with the high-temperature branch is almost 20 times greater than the value for the low-temperature branch. This is believed to be associated with the cutting of β_2' and β particles by dislocations where the Burgers vector of the dislocation is perpendicular to the slip plane of the particles. Fig. 16 shows that the $(2\bar{1}\bar{1}0)$ slip plane of β_2' is perpendicular to the basal plane of the Mg matrix. The slip plane of the β is also perpendicular to the Mg basal plane. It is apparent from fig. 5 that the β and β_2' particles are 10 to 20 times larger than the thickness of the β_1' precipitates. It is believed that this is the cause of the high-temperature branch having an activation energy twenty times that of the low-temperature branch. The GPI zones in Al–3.9 wt % Cu alloy [11] are a similar case. The activation volume for the high-temperature branch can be further rationalised by the smaller density of either β_2' or β particles compared to β_1'. The separate contributions of β_2' and β, however cannot be delineated with presently available theories. It can only be pointed out that the temperature-dependence of crss, is greater than that of the shear modulus and that some transmission-electron micrographs seemed to show particle cutting. On this basis the above mechanistic conclusions seem reasonable.

In single crystals of Al–3.9 wt % Cu the rate of work-hardening was found to be $G/500$ at 4.2° K when precipitate cutting is involved and $G/10$ when Orowan's mechanism is in operation [11]. Thus, if dislocations bow out between precipitates, it might reasonably be expected that the rate of work-hardening be as much as fifty times larger than if dislocations shear through the precipitates. Fig. 10 shows that at room temperature the fully aged and overaged crystals have the *same* rate of work-hardening as that of the quenched condition. This is also true at 77° and 4.2° K. Additional evidence that dislocations cut the precipitates in the overaged condition was noted by transmission electron microscopy of a sample deformed by handling during preparation.

Thus all the experimental results indicate that the strengthening in the overaged condition also appears to be due to the shearing of particles, in this case the β_1', β_2' and β, by dislocations.

Acknowledgement

The authors are indebted to Dr A. Bornemann and Dr H. Herman for their most helpful assistance and to Dr P. S. Nicholson for many helpful suggestions on the original manuscript.

References

1. J. G. BYRNE, *Acta Met.* **11** (1963) 1023.
2. R. De LUCA, and J. G. BYRNE, AIME Symposium on Work Hardening (1968) (Gordon and Breach, New York).
3. *Idem*, Inter. Conf. on the Strength of Metals and Alloys, Tokyo (1967).
4. C. S. ROBERTS, "Magnesium and Its Alloys" (Wiley, New York, 1960).
5. J. GALLOT, Ph.D. Thesis, Université de Rouen (1966).
6. D. C. JILLSON, *J. Metals* **188** (1950) 1005.
7. J. S. CHUN, A. BORNEMANN, and J. G. BYRNE, *Brit. J. Appl. Phys.* **2** (1969), 909.
8. J. B. CLARK, *Acta Met.* **13** (1965) 1281.
9. R. De LUCA, Ph.D. Thesis, Stevens Institute of Technology (1966).
10. J. V. SHARP, Ph.D. Thesis, University of Oxford (1964).
11. J. G. BYRNE, M. E. FINE, and A. KELLY, *Phil Mag.* **6** (1961) 1119.
12. N. F. MOTT, and F. R. N. NABARRO, Rep. Conf. Strength of Solids (Phys. Soc., 1948) p. 1.
13. J. C. FISHER, *Acta Met.* **2** (1954) 9.
14. H. SUZUKI, *Sci. Prep. Res. Inst. Tohoku University* **A1** (1952) 183.
15. J. FRIEDEL, NPL Symposium on the Relation Between the Structure and Mechanical Properties of Metals (HMSO, 1963) p. 261.
16. A. H. COTTRELL, "Dislocations and Plastic Flow in Crystals" (Oxford University Press, 1953).
17. R. L. FLEISCHER, NPL Symposium in the Relation Between the Structure and Mechanical Properties of Metals (HMSO, 1963) p. 410.
18. N. F. MOTT, *Phil. Mag.* **1** (1956) 568.
19. A. SEEGER, Proc. 2nd International Conf. on Peaceful Uses of Atomic Energy (1958) p. 998.
20. A. KELLY and P. B. NICHOLSON, *Progr in Mat. Sci.* **10** (1963) 344.
21. R. De LUCA, and J. G. BYRNE, *Acta Met.* **13** (1965) 187.
22. W. DESORBO, H. N. TREAFTIS, and D. TURNBULL, *ibid* **6** (1958) 401.
23. T. FEDERIGHI, *ibid* **6** (1958) 379.
24. D. TURNBULL and H. S. ROSENBAUM, *ibid* **6** (1958) 653.
25. P. B. HIRSCH and A. KELLY, *Phil. Mag.* **12** (1965) 881.
26. P. B. PRICE, "Electron Microscopy and Strength of Crystals" (Wiley, New York and London, 1963) p. 41.
27. A. SEEGER, S. MADER, and H. KRONMÜLLER, "Electron Microscopy and Strength of Crystals" (Wiley, New York and London, 1963) p. 665.
28. H. CONRAD, and W. D. ROBERTSON, *Trans. AIME* **209** (1957) 425.
29. J. S. CHUN and J. G. BYRNE, *Phil. Mag.* (1969) to be published.
30. E. OROWAN, A Symposium on Internal Stresses (1948) (Institute of Metals, London) p. 45.